Signal-free Path-free Intersection Control for Connected Vehicles under Automated Driving

Signal-free Path-free Intersection Control for Connected Vehicles under Automated Driving

Elham Ahmadi, Alireza Olama, Rodrigo Castelan Carlson, *Senior Member, IEEE,* Eduardo Camponogara

***Abstract*—We present a method for the signal-free path-free intersection control (SPIC) problem which involves coordinating connected vehicles under automated driving (CVAD) at urban intersections. A receding horizon planner is formulated as an extension of the nonlinear model predictive contouring control (NMPCC), referred to as ENMPCC. The ENMPCC method involves the inclusion of additional cost terms, traffic safety constraints, and the generation of multiple time-independent reference paths. The proposed method drops the constraints on the allowed paths within the intersection. This allows CVAD to move freely along optimal trajectories and paths, maximizing efficiency without compromising safety. Utilizing a polytopic representation of each CVAD and incorporating duality theory to formulate collision avoidance constraints, our method enables optimal and collision-free traversal of CVAD within the intersections. We demonstrate the proposed method in an urban driving scenario involving both straight and turning movements at an intersection. In comparison to the conventional path-based (lane-based) driving of the CVAD, our method shows a better use of intersection space resulting in lower travel time and fuel consumption as demonstrated through our simulation results.**

***Index Terms*—Traffic control, connected vehicles under automated driving, model predictive contouring control, collision avoidance, urban intersections.**

TABLE I
LIST OF ACRONYMS

CCP	Contouring Control Problem
CG	Center of Gravity
CVAD	Connected Vehicles under Automated Driving
ENMPCC	Extended Nonlinear Model Predictive Contouring Control
LTV	Linear Time-Varying
LTV-ENMPCC	Linear Time-Varying Extended Nonlinear Model Predictive Contouring Control
MPC	Model Predictive Control
NLP	NonLinear Programming
NMPCC	Nonlinear Model Predictive Contouring Control
NOCP	Nonlinear Optimal Control Problem
SPIC	Signal-free Path-free Intersection Control
TTS	Total Time Spent

I. Introduction

URBAN intersections are a crucial part of the transportation system. The shared road space is subject to vehicles with different origins and destinations, leading to conflicts. Conventional traffic control systems manage these conflicts by defining a limited set of allowed paths and associated traffic movements. Right of way for each movement or set of non-conflicting movements are granted sequentially by traffic signals [1]. With the advent of connected vehicles under automated driving (CVAD), new methods for coordinating traffic at signal-free intersections have been developed, aiming to improve traffic efficiency by enabling shorter headways and eliminating lost time [2]–[4]. However, most of these methods still rely on the concept of traffic movements and associated predetermined paths, limiting the use of intersection space [5].

To increase the use of intersection space, researchers proposed to expand the number of allowed paths for specific traffic movements [6]. Vehicles on any lane were allowed to turn in any direction, at the cost of increasing the number of conflicts inside an intersection. Another work developed a hybrid cooperative approach consisting of microscopic-level virtual platooning control and macroscopic-level traffic flow regulation for controlling signal-free multi-lane intersections in a connected autonomous vehicle traffic environment [7]. A decentralized two-level optimal framework is developed in [8] to address the problem of coordinating platoons of connected and automated vehicles crossing a signal-free intersection with the objective of minimizing travel delay and fuel consumption. They investigated the effect of platooning by considering platoons of varying sizes while crossing the intersection. Additionally, a different organization of traffic at intersections that allows for real-time lane direction reversal was proposed by Stevanovic et al. [9]. Although the left- and right-turning movements traverse the intersection without any conflicts, the through vehicles are still required to reserve time-space slots to avoid a collision. It was shown that the method outperformed conventional driving. However, even with these strategies, the number of admissible paths remains restricted, constraining the achievable capacity at the intersection.

A better use of the intersection space to improve overall traffic efficiency can be accomplished by leveraging the potential of the CVAD to enable path-free traversing at a signal-free intersection. There are a variety of names used in the literature for this type of intersection; *intersection plaza* [5], [10], *lane-free intersection* [11], [12], *path-free intersection* [13], [14],

This work was funded in part by Fundação de Amparo à Pesquisa e Inovação do Estado de Santa Catarina (FAPESC) under grant 2021TR2265; by The Brazilian Agency for Higher Education, under PROEX and the project PrInt CAPES-UFSC "Automation 4.0"; and by the National Council for Scientific and Technological Development. (*Corresponding author: Elham Ahmadi*)

E. Ahmadi was with the Post-graduate Program in Automation and Systems Engineering (PGEAS), Federal University of Santa Catarina (UFSC), Florianópolis-SC, Brazil 88.040-900, and now is with the School of Technology and Innovations, University of Vaasa, Finland (e-mail: elham.ahmadi@posgrad.ufsc.br, elham.ahmadi@uwasa.fi)

A. Olama was with the PGEAS, UFSC, and now is with the Department of Information Technology, Åbo Akademi University, Finland (e-mail: alireza.olama@posgrad.ufsc.br, alireza.olama@abo.fi).

R. C. Carlson and E. Camponogara are with the PGEAS, UFSC (e-mail: rodrigo.carlson@ufsc.br, eduardo.camponogara@ufsc.br).

among others. We refer to [15] for a related discussion. In any case, the intersection transforms into a boundary-constrained free space, where free paths are permitted on the condition that the resulting trajectories do not collide. This enables a better use of the intersection space and increased capacity.

An early work proposed a centralized control strategy for connected automated vehicles crossing a lane-free intersection, which involves a nonlinear optimal control problem (NOCP) to compute possible trajectories offline based on pre-defined formations at the intersection's approaches [11]. The vehicles are then guided through a sequence of buffers to reach the intersection matching one of the formations that were computed offline. Afterward, the same problem was revisited and the intersection was microscopically described as a free space and the problem was simplified by fixing the time that a vehicle takes to traverse the intersection [16]. However, the complexity of the problem makes it challenging to solve numerically due to the high-dimensional collision avoidance constraints and the nonlinearity of the model.

Other NOCP-based approaches to coordinate the CVAD at signal-free path-free intersections were able to obtain efficient collision-free trajectories by taking advantage of free paths and better use of the available space. One approach reduced the NOCP to a nonlinear programming (NLP) problem through the use of either finite Fourier series [5] or Bézier curves [10] and discretization. A minimum-time NOCP formulation was also attempted [12]. The non-convex collision avoidance constraints were reformulated by the use of the dual problem theory. This approach reduced the intersection crossing time, but the scale of collision avoidance constraints made the method computationally expensive. These NOCP-based methods [5], [10], [12] are limited because they do not take into account the continuous arrival of vehicles, are conducted offline, require prior knowledge of the initial and final states of the CVAD, and impose the same travel times on all CVAD. As a result, these methods do not address a realistic problem.

To address the limitations of previous works, other works [13], [14], [17] proposed a receding horizon approach based on optimal control to coordinate the vehicles at path-free signal-free urban intersections. The first [13], used a nonlinear model predictive control (MPC) to coordinate straight movements of CVAD in the intersection based on the work by [18]. The method was compared to the path-based optimal arrival time strategy [19]. The second and third [14], [17], formulated the CVAD coordination in the intersection as a nonlinear model predictive contouring control (NMPCC) problem [20], [21]. Both works used the Euclidean distance between CVAD to avoid collisions, resulting in non-convex optimization problems that are challenging to solve. Another work proposed a strategy employing a NOCP for every connected and automated vehicle traversing a lane-free ring-road, and conducted simulations to assess its efficacy [22]. Moreover, [23] proposed a method to control automated vehicles in large lane-free roundabouts. It used offline-computed movement corridors and feedback controllers to guide vehicles to their destinations while avoiding collisions and minimizing trip distances.

In this paper, we propose a signal-free path-free intersection control (SPIC) problem to coordinate each CVAD at urban intersections. SPIC enables smooth and safe movement of each vehicle without the need for traditional signals or predefined paths, allowing for adaptable driving behaviors and optimal use of intersection space. An extended and tailored NMPCC method is then introduced to address the solution of the SPIC problem which we refer to as extended NMPCC (ENMPCC). The ENMPCC method generates collision-free and optimal CVAD trajectories based on time-independent and continuously differentiable reference paths, with focus on maximizing progress along the paths. To guarantee collision avoidance, the areas occupied by CVAD are modeled as polytopic sets and each set should maintain a minimum safe distance from the other sets. To enhance numerical efficiency, we incorporate a linear time-varying (LTV) model, used in standard NMPCC, into the ENMPCC problem, yielding LTV-ENMPCC.

The contributions are summarized as follows:

- The SPIC problem formulation enables path-free traversing of CVAD at signal-free intersections for the efficient use of the intersection space. Compared to [5], [10], [12], our formulation explores the full space of the intersection for any feasible arrival of vehicles without imposing final states and identical travel times for the vehicles.
- The ENMPCC method, which solves the SPIC problem, is suitable for optimal, smooth, and collision-free trajectory generation of CVAD in an intersection.
- Incorporation of continuous arrivals of vehicles at the intersection as done by [24]. However, we employ an online optimization approach. Previous signal-free path-free (lane-free) intersection coordination methods [5], [10], [12], considered one instance of the problem at a time with a fixed number of vehicles, each with a given initial state, and these vehicles are controlled on the road.
- Offline generation of multiple time-independent reference paths to cover all possible movements, including straight and turning movements, in an intersection in contrast to [13], [14] that considered a subset of all possible movements.
- Analysis and comparison with the conventional path-based (lane-based) driving approach through numerical simulation of various traffic scenarios.

This paper is organized as follows. Section II models the system, including the intersection, vehicle, path, and constraints. Section III presents the formulation of the SPIC problem and the ENMPCC method. Section IV presents the simulation results. The conclusions are presented in Section V.

II. System Modeling

In this section, we introduce the intersection, the vehicle, and the reference path models, and practical safety constraints.

A. Intersection Plaza Model

We consider a Plaza [5] as an empty space free of movement-related horizontal markings or structural restrictions, except for its boundaries. CVAD operating within the Plaza take advantage of unrestricted flexibility in moving freely on the approaches in order to either avoid potential collisions with other CVAD or to expedite their traversal. The

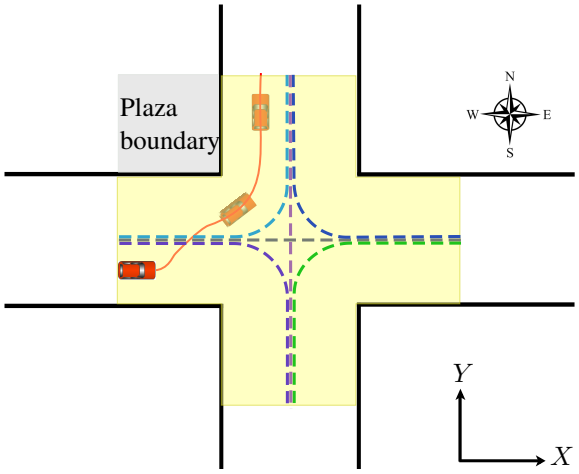

Fig. 1. A four-leg signal-free intersection as a plaza (yellow area) with one CVAD traversing on a path-free; the solid black lines mark the plaza boundaries and the colored dashed lines show the different reference paths.

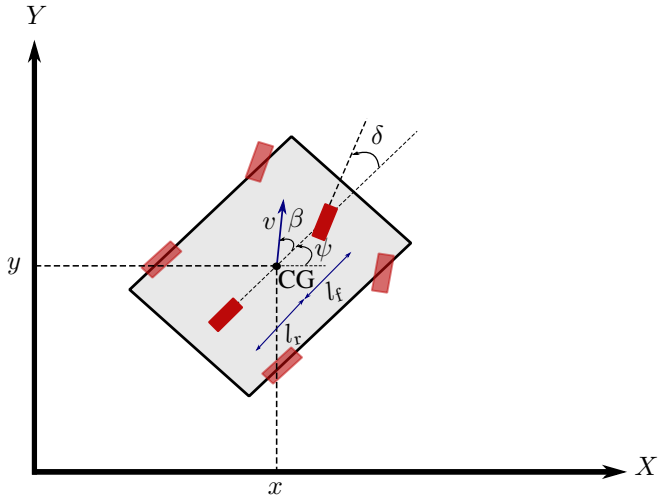

Fig. 2. Kinematic bicycle model with the left and right wheels lumped into single wheels in the middle of the vehicle's axles; x and y, respectively, the longitudinal and lateral position of each CVAD, ψ the orientation, v the speed, β the slip angle at the center of gravity (CG) of the vehicle, and δ is the front wheel steering angle; the distances from the front and rear axles to the CG are l_{f} and l_{r}.

configuration of a Plaza may differ concerning the number of roads that intersect and their geometry. We focus on urban intersections modeled as Plazas, although other types of intersections may be handled by the same method.

To introduce the concept, we choose a four-leg intersection depicted in Fig. 1. The yellow area with boundaries delimited by black lines is the Plaza. The X and Y axes denote the central lines of the Plaza on the Cartesian coordinate system. In the figure, a vehicle is traversing from its initial position toward its destination. Within the Plaza, the vehicle is free to adjust its trajectory, shown by the solid red line, without being bound to predetermined paths or traffic lanes. Consequently, if the vehicle's trajectory does not intersect with the trajectories of other vehicles in the Plaza at the same location and time, there is no collision. In other words, a minimum safe distance is maintained between each vehicle and the Plaza boundaries, as well as between every two vehicles at all times.

This paper is based on the following assumptions: 1) CVAD communicate their states and driving intentions; 2) only CVAD operate in the Plaza; 3) upstream and downstream of the Plaza the CVAD operate within designated lanes as in conventional driving. Assumption 3 can be relaxed if we assume there is a system interfacing with upstream and downstream roads.

B. Vehicle Model

There are various models to describe a vehicle's dynamics, from the simple unicycle model [25] to sophisticated vehicle models [26]. We model each vehicle within the Plaza by using a nonlinear kinematic bicycle model [27]. This model lumps the left and right wheels into a pair of single wheels in the middle of the vehicle's axles, see Fig. 2. The discretized bicycle model of a vehicle is given by [27]:

$$
\begin{aligned}
x_{i,k+1} &= x_{i,k} + \Delta t\, v_{i,k} \cos(\psi_{i,k} + \beta_{i,k}),\\
y_{i,k+1} &= y_{i,k} + \Delta t\, v_{i,k} \sin(\psi_{i,k} + \beta_{i,k}),\\
\psi_{i,k+1} &= \psi_{i,k} + \Delta t\, \frac{v_{i,k} \sin(\beta_{i,k})}{l_{\mathrm{r},i}},\\
v_{i,k+1} &= v_{i,k} + \Delta t\, a_{i,k},\\
\beta_{i,k} &= \tan^{-1}\left(\frac{l_{\mathrm{r},i}}{l_{\mathrm{f},i} + l_{\mathrm{r},i}} \tan(\delta_{i,k})\right),
\end{aligned}
\tag{1}
$$

with k the discrete time index, and Δt (s) the time step. Each vehicle is identified by its index $i \in \mathcal{V} = \{1, 2, \ldots, N_{\mathrm{v}}\}$ with N_{v} as the number of vehicles. The i-th vehicle state vector is $\mathbf{x}_{i,k} = [x_{i,k}, y_{i,k}, \psi_{i,k}, v_{i,k}]^{\top}$, in which $x_{i,k}$ (m) and $y_{i,k}$ (m) are the longitudinal and lateral position of each CVAD, respectively, $\psi_{i,k}$ (rad) is the orientation, and $v_{i,k}$ (m/s) and $\beta_{i,k}$ (rad) are the speed and the slip angle at the center of gravity (CG) of the vehicle. The i-th vehicle control vector is $\mathbf{u}_{i,k} = [a_{i,k}, \delta_{i,k}]^{\top}$, in which $a_{i,k}$ (m/s^2) is the acceleration and $\delta_{i,k}$ (rad) is the front wheel steering angle of the vehicle. The distances from the front and rear axles to the CG of the i-th vehicle are $l_{\mathrm{f},i}$ (m) and $l_{\mathrm{r},i}$ (m), respectively.

This kinematic bicycle model is a suitable choice for our Plaza application; the model can be implemented in low-speed vehicles commonly found at intersections, allows for designing controllers for stop-and-go scenarios frequently encountered in urban driving, and is less computationally demanding than methods that employ vehicle tire models [27].

C. Reference Path Model

We use the road center lines as reference paths. Six different bidirectional paths cover all possible twelve origin-destinations at the intersection plaza in Fig. 1. Each reference path is then followed by the vehicles according to their traversal.As an example, the light blue dashed line shows the turning reference path for the vehicle approaching the plaza from the west

intended to make a left turn. The other reference paths follow a similar description for the remaining directions.

The goal is to control the motion of the CVAD along reference paths while minimizing the distance between the current position of the CVAD and the reference path, which is known as the contouring control problem (CCP) [28]. In this work, we acknowledge the need for significant deviations from the reference path as long as the CVAD trajectories are collision-free and within the intersection boundaries.

Next, we review some concepts of the CCP, including the parameterization of the reference path and the definition of the path error measures based on two orthogonal components, the lateral (contouring) and longitudinal (lag) errors [20].

1) Reference Path Parameterization: each CVAD at position $\mathbf{p}_k = (x_k,\, y_k)$ follows a continuously differentiable and time-independent reference path $\mathbf{p}^{\mathrm{ref}}(\theta) = (x^{\mathrm{ref}}(\theta), y^{\mathrm{ref}}(\theta))$, parameterized by the path parameter θ [21], [29].

2) Lateral and Longitudinal Errors: contouring accuracy is measured by the lateral error, that is the shortest distance of the actual position of the vehicle $\mathbf{p}_k$ from the reference path, $\mathbf{p}^{\mathrm{ref}}(\theta)$, see Fig. 3. The value of the path parameter for which the distance between $\mathbf{p}_k$ and $\mathbf{p}^{\mathrm{ref}}(\theta)$ is minimal can be obtained by the following projection problem:

$$\min_{\theta} \ \|\mathbf{p}_k - \mathbf{p}^{\mathrm{ref}}(\theta)\|_2, \tag{2}$$

where the minimizer at time step k is θ_k as shown in Fig. 3. The lateral error is then given by [20], [28]:

$$E_k^{\mathrm{c}} = \sin(\phi(\theta_k))(x_k - x^{\mathrm{ref}}(\theta_k)) - \cos(\phi(\theta_k))(y_k - y^{\mathrm{ref}}(\theta_k)), \tag{3}$$

where $\phi(\theta_k)$ is the tangent angle to the reference path with respect to the x axis and given as:

$$\phi(\theta_k) = \arctan\left(\frac{\nabla y^{\mathrm{ref}}(\theta_k)}{\nabla x^{\mathrm{ref}}(\theta_k)}\right), \tag{4}$$

with $\nabla y^{\mathrm{ref}}(\theta_k) = dy^{\mathrm{ref}}(\theta)/d\theta\big|_{\theta=\theta_k}$ and $\nabla x^{\mathrm{ref}}(\theta_k) = dx^{\mathrm{ref}}(\theta)/d\theta\big|_{\theta=\theta_k}$.

However, given that (2) is an optimization problem itself, this formulation of lateral error is not appropriate for use in an online optimization problem. Then, an approximation $\hat{\theta}_k$ of θ_k was introduced with dynamics [20], [30]:

$$\hat{\theta}_{k+1} = \hat{\theta}_k + \Delta t\, \nu_k, \ \ \nu_k \in [0, \nu_{\max}], \ \nu_{\max} > 0, \tag{5}$$

where $\hat{\theta}_k$ is the approximated value of the path parameter at time k that can be interpreted as the vehicle progress along the reference path, ν_k is a virtual input that controls the evolution of $\hat{\theta}_k$, and $\nu_{\max}$ is a maximum value for the virtual input.

The optimal path parameter θ_k and its approximation $\hat{\theta}_k$ are linked by introducing the longitudinal error $E_k^{\mathrm{l}} = \|\theta_k - \hat{\theta}_k\|$. The longitudinal error is also approximated since θ_k is not known at the optimization time. Consequently, the approximated lateral error ($\hat{E}_k^{\mathrm{c}}$) and approximated longitudinal error ($\hat{E}_k^{\mathrm{l}}$) are defined as follows:

$$\hat{E}_k^{\mathrm{c}} = \sin(\phi(\hat{\theta}_k))(x_k - x^{\mathrm{ref}}(\hat{\theta}_k)) - \cos(\phi(\hat{\theta}_k))(y_k - y^{\mathrm{ref}}(\hat{\theta}_k)), \tag{6}$$

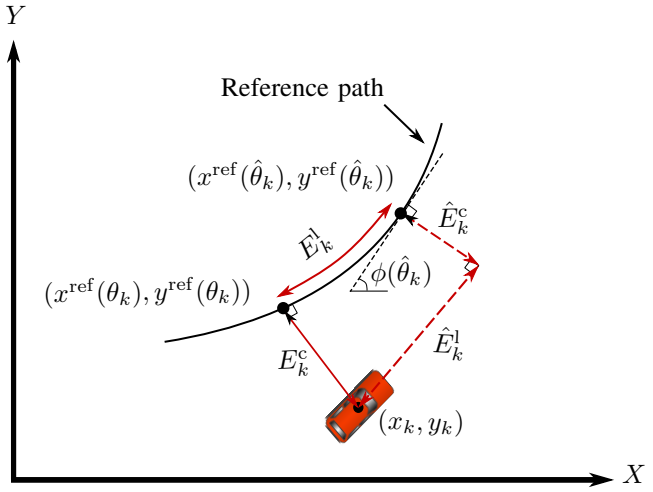

Fig. 3. A reference path corresponding to the center line of a road used for computing the vehicles' progress; lateral error (E_k^{c}) and longitudinal error (E_k^{l}), shown in solid red lines and their approximation $\hat{E}_k^{\mathrm{c}}$ and $\hat{E}_k^{\mathrm{l}}$ shown in dashed red lines. If $\hat{E}_k^{\mathrm{l}}$ is zero, then E_k^{l} is also zero and therefore $\hat{\theta}_k$ is equal to θ_k.

$$\hat{E}_k^{\mathrm{l}} = -\cos(\phi(\hat{\theta}_k))(x_k - x^{\mathrm{ref}}(\hat{\theta}_k) - \sin(\phi(\hat{\theta}_k))(y_k - y^{\mathrm{ref}}(\hat{\theta}_k)), \tag{7}$$

where $\phi(\cdot)$ is defined in (4). It can be seen in Fig. 3 that $\theta_k \approx \hat{\theta}_k$ if $\hat{E}_k^{\mathrm{l}} \approx 0$.

D. Vehicle's Kinematic Constraints

To guarantee that vehicles remain within their dynamic limitations, the constraints below are enforced for each CVAD:

$$v_{\min} \le v_{i,k} \le v_{\max},\ \delta_{\min} \le \delta_{i,k} \le \delta_{\max},\ a_{\min} \le a_{i,k} \le a_{\max}, \tag{8}$$

where $v_{\min}$, $v_{\max}$, $\delta_{\min}$, $\delta_{\max}$, $a_{\min}$, and $a_{\max}$ are the lower and upper bounds of speed, steering angle, and acceleration.

E. Plaza Boundary Constraints

The optimization problem must satisfy constraints to prevent the i-th CVAD from violating the intersection boundaries. Therefore, a well-defined circle with the center point moving along the reference path $\mathbf{p}^{\mathrm{ref}} = [x^{\mathrm{ref}}(\hat{\theta}_{i,k}), y^{\mathrm{ref}}(\hat{\theta}_{i,k})]^\top$ is used to allow each CVAD to traverse only within it as illustrated in Fig. 4. The Plaza boundaries constraints are then defined as the following convex constraints [18]:

$$\mathrm{dist}(\mathbf{p}_i,\, \mathbf{p}^{\mathrm{ref}}) \le \frac{w_{\mathrm{r}} - w_{\mathrm{v},i}}{2}, \tag{9}$$

where $\mathrm{dist}(\mathbf{p}_i,\, \mathbf{p}^{\mathrm{ref}})$ is the Euclidean distance between the current position of the i-th vehicle and the point $\mathbf{p}^{\mathrm{ref}}$, with w_{r} being the road width.

F. Vehicle-to-Vehicle (V2V) Collision Avoidance Constraints

To avoid collisions between two CVAD, each CVAD is modeled as a polytopic set $\mathcal{P}$, which is a bounded intersection of a finite number of half-spaces. The initial pose of each CVAD is represented by a two-dimensional rectangular polytope $\tilde{\mathcal{P}}_i$ as (see Fig. 4) [31]:

$$\tilde{\mathcal{P}}_i = \{\mathbf{p}_i \in \mathbb{R}^2 \mid \tilde{\mathbf{A}}_i\, \mathbf{p}_i \le \tilde{\mathbf{b}}_i\}, \tag{10}$$

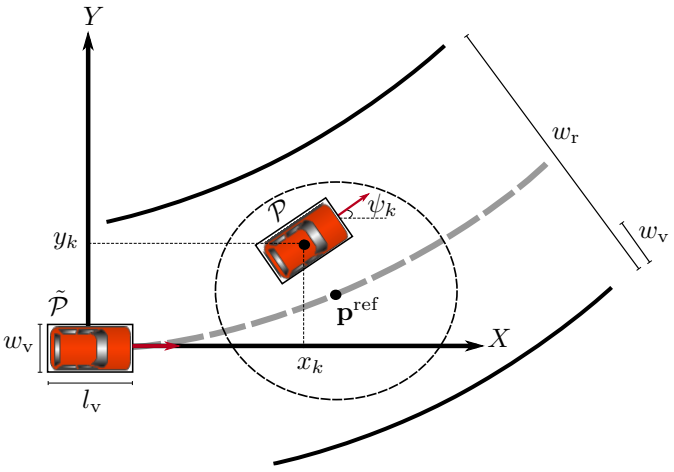

Fig. 4. Schematic of a road; the thick black curves are the left and right boundaries of the road and the dashed gray curve is a reference path; the dashed circle around point $\mathbf{p}^{\mathrm{ref}} = [x^{\mathrm{ref}}, y^{\mathrm{ref}}]^\top$ shows the area within which the vehicle satisfies the boundary constraint that forces the vehicle to remain within the road boundaries. $\mathcal{P}$ is the polytopic representation of the vehicle and its transformation from $\tilde{\mathcal{P}}$ to $\mathcal{P}$ with ψ_k as the vehicle orientation.

where $\mathbf{p}_i = [x_{i,k}, y_{i,k}]^\top$, $\tilde{\mathbf{A}}_i = [\mathbf{I}_{2\times 2}, -\mathbf{I}_{2\times 2}]^\top$, and $\tilde{\mathbf{b}}_i = [l_{\mathrm{v},i}/2, w_{\mathrm{v},i}/2, l_{\mathrm{v},i}/2, w_{\mathrm{v},i}/2]^\top$ with $l_{\mathrm{v},i}$ being the length and $w_{\mathrm{v},i}$ the width of the i-th CVAD. As each CVAD i moves along the road, polytope $\tilde{\mathcal{P}}_i$ undergoes affine transformations including rotation and translation. Hence, the transformed polytope $\mathcal{P}_i$ is a function of the states and defined as:

$$\mathcal{P}_i(\mathbf{x}_{i,k}) = \{\mathbf{p}_i \in \mathbb{R}^2 \,|\, \mathbf{A}_i(\mathbf{x}_{i,k})\,\mathbf{p}_i \leq \mathbf{b}_i(\mathbf{x}_{i,k})\}, \tag{11}$$

where $\mathbf{A}_i(\mathbf{x}_{i,k}) = \tilde{\mathbf{A}}_i \begin{bmatrix} \cos(\psi_{i,k}) & -\sin(\psi_{i,k}) \\ \sin(\psi_{i,k}) & \cos(\psi_{i,k}) \end{bmatrix}$ and $\mathbf{b}_i(\mathbf{x}_{i,k}) = \tilde{\mathbf{b}}_i + \mathbf{A}_i(\mathbf{x}_{i,k})\,\mathbf{p}_i$. This representation is time-varying and is a function of the vehicle states. For clarity and simplicity, in the following, we consider $\mathcal{P}_i = \mathcal{P}_i(\mathbf{x}_{i,k})$, $\mathbf{A}_i = \mathbf{A}_i(\mathbf{x}_{i,k})$, and $\mathbf{b}_i = \mathbf{b}_i(\mathbf{x}_{i,k})$.

To prevent collisions, the intersection of the polytopic sets of vehicles $i, j \in \mathcal{V}$, and $i < j$, should be avoided, that is, $\mathcal{P}_i \cap \mathcal{P}_j = \emptyset$. $\mathcal{P}_i$ and $\mathcal{P}_j$ being the i-th and j-th CVAD polytopes, respectively. This results in a non-convex and non-smooth problem that is difficult to solve [32]. In the next section, we address this issue by reformulating $\mathcal{P}_i \cap \mathcal{P}_j = \emptyset$ to a smooth and differentiable optimization problem.

III. SPIC Problem Formulation

The primary objective of this work is to develop an optimization-based control approach for coordinating vehicles at an intersection. In this section, we introduce the basic formulation of the SPIC problem which is formulated as an extended and tailored NMPCC method, referred to as the extended NMPCC (ENMPCC). By employing linear time-varying (LTV) approximation obtained through the linearization of nonlinear functions and leveraging duality theory for V2V constraints, we finally introduce the final formulation of the SPIC as an LTV-ENMPCC optimization problem.

A. Extended Nonlinear Model Predictive Contouring Control

NMPCC [20] is a control strategy that combines the principles of path-following control [33] with the concept of contouring control [34] and model predictive control [35]. The objective of NMPCC is to minimize the projected distance between the current position of a tool or object and a reference path while maximizing its progress along the path. NMPCC offers the advantage of combining both path planning and path following in a single nonlinear optimization problem through the application of contouring control. In contrast to the state-of-the-art motion planning techniques that involve a two-level optimization process, where an upper-level optimizer generates time-dependent trajectories and a lower-level optimizer tracks the generated trajectory accurately [36], [37], the NMPCC combines these levels into a single optimal control problem.

In the following, the standard NMPCC formulation is extended to enable its application to the SPIC problem. The ENMPCC method involves the inclusion of additional cost terms, such as fuel consumption (due to acceleration) or driving comfort (due to steering angle), and additional reference paths to cover all possible vehicle paths at the intersection plaza. Compared to the standard formulation, we incorporate V2V constraints to prevent potential vehicle collisions. Moreover, we impose intersection boundary constraints to restrict vehicle movements within intersection boundaries. This becomes especially crucial when the longitudinal cost, q_{c}, is chosen small, which allows vehicles to deviate from the reference paths as needed to avoid potential collisions and/or to expedite their traverse. While NMPCC has been applied to car racing [21], winding roads [18], parallel autonomy for self-driving cars [38], and drones [39], this work applies ENMPCC to a signal-free path-free urban intersection, which is more challenging.

B. Objective Function

In this problem, we would like to minimize the lateral and longitudinal errors and maximize the vehicles progress along the reference paths while penalizing the control inputs for each CVAD in the intersection plaza. Given $\hat{\mathbf{E}}_k = [\hat{E}_k^{\mathrm{c}}, \hat{E}_k^{\mathrm{l}}]^\top$, the objective function is:

$$J = \hat{\mathbf{E}}_k^\top \mathbf{Q} \hat{\mathbf{E}}_k + \nu_k^\top r_\nu \nu_k - q_\theta \hat{\theta}_k + \mathbf{u}_k^\top \mathbf{R} \mathbf{u}_k, \tag{12}$$

where $\mathbf{Q} = \begin{bmatrix} q_{\mathrm{c}} & 0 \\ 0 & q_{\mathrm{l}} \end{bmatrix}$ and $\mathbf{R} = \begin{bmatrix} r_{\mathrm{v}} & 0 \\ 0 & r_\delta \end{bmatrix}$ are weighting matrices, $q_{\mathrm{c}} > 0$, $q_{\mathrm{l}} > 0$, $r_\nu > 0$, and $q_\theta > 0$ are lateral error, longitudinal error, virtual input, and progress cost weights, respectively, and $r_{\mathrm{v}} > 0$ and $r_\delta > 0$ are, respectively, the weights on the acceleration and steering angle of each vehicle. The appropriate tuning of these weights allows for a trade-off between contouring accuracy and progress along the reference paths. In this application, it is desirable to sacrifice contouring accuracy to allow vehicles to traverse the path as fast as possible and make better use of the intersection space.

C. Basic Formulation of the SPIC Problem

In this section, we introduce the SPIC problem formulation as the following ENMPCC optimization problem that computes optimal and collision-free trajectories for all the CVAD in the intersection plaza:

$$\min_{\substack{\mathbf{u}_{i,\cdot|k},\\ \nu_{i,\cdot|k},\forall i}} \quad \sum_{i=1}^{N_\mathrm{v}} \Bigg(\sum_{t=k}^{k+N_\mathrm{h}} \hat{\mathbf{E}}_{i,t}^\top \mathbf{Q} \hat{\mathbf{E}}_{i,t} - q_\theta \hat{\theta}_{i,t} + \sum_{t=k}^{k+N_\mathrm{h}-1} \mathbf{u}_{i,t}^\top \mathbf{R} \mathbf{u}_{i,t} + \nu_{i,t}^\top r_\nu \nu_{i,t} \Bigg) \tag{13a}$$

$$\text{s.t.} \quad \mathbf{x}_{i,t+1|k} - \mathbf{f}(\mathbf{x}_{i,t|k}, \mathbf{u}_{i,t|k}) = \mathbf{0}, \tag{13b}$$

$$\hat{\theta}_{i,t+1|k} = \hat{\theta}_{i,t|k} + \Delta t\, \nu_{i,t|k}, \tag{13c}$$

$$\mathbf{x}_{i,0|k} - \mathbf{x}_{i,k} = \mathbf{0},\ \hat{\theta}_{i,0|k} - \hat{\theta}_{i,k} = 0, \tag{13d}$$

$$\mathbf{x}_{i,t|k} \in \mathcal{X},\ \mathbf{u}_{i,t|k} \in \mathcal{U},\ \nu_{i,t|k} \in [0, \nu_{\max}], \tag{13e}$$

$$\|\mathbf{p}_{i,t|k} - \mathbf{p}^{\mathrm{ref}}\|_2 \leq \frac{w_\mathrm{r} - w_{\mathrm{v},i}}{2}, \tag{13f}$$

$$\mathcal{P}(\mathbf{x}_{i,t|k}) \cap \mathcal{P}(\mathbf{x}_{j,t|k}) = \emptyset. \tag{13g}$$

where subscript i refers to i-th CVAD and N_h is the prediction horizon. This problem is a multi-objective optimization problem, with (13a) representing the objective function as defined in (12). In (13b), the function $\mathbf{f}(\cdot)$ represents the nonlinear model of each CVAD as defined in (1). Equation (13c) represents the vehicle's progress in which $\hat{\theta}_i$ and ν_i are, respectively, an additional state variable and an additional control variable. The state and input feasible sets are respectively denoted by $\mathcal{X}$ and $\mathcal{U}$, which show the state and control input constraints as defined in (8). Additionally, constraints (13f) and (13g) represent the intersection plaza boundary constraints and the V2V collision avoidance constraints, respectively.

D. Linear Time-Varying (LTV) Implementation

Problem (13) is an NMPCC problem that is solved online at each time step. The computational cost associated with solving this problem can be high. The linear time-varying approximation of the nonlinear kinematic bicycle model as well as of the lateral and longitudinal errors is used to construct a tractable optimization problem [40]. Each nonlinear function is linearized around the output of the last solution of the optimal control problem over a shifted horizon, except for the first and the last steps. The state of the first step is measured. The last step was not predicted in the previous solution. Thus, the system is simulated for one time step assuming that the input is the same as in the second to last step.

1) LTV Approximation of the Vehicle Model: The kinematic bicycle model (1) is approximated by first-order Taylor series expansion around the predicted state's trajectory ($\bar{\mathbf{x}}_k = [\bar{x}_k, \bar{y}_k, \bar{\psi}_k, \bar{v}_k]^\top$) and control inputs ($\bar{\mathbf{u}}_k = [\bar{a}_k, \bar{\delta}_k]^\top$) computed at the previous time step as:

$$\bar{\mathbf{x}}_{k+1} = \mathbf{A}_k \bar{\mathbf{x}}_k + \mathbf{B}_k \bar{\mathbf{u}}_k + \mathbf{d}_k, \tag{14}$$

where $\mathbf{A}_k$ and $\mathbf{B}_k$ are suitable matrices and $\mathbf{d}_k$ is a constant vector formed through linearization of model (1) at step k.

2) LTV Approximation of Lateral and Longitudinal Errors: The lateral and longitudinal errors (6) and (7) are approximated by linear functions over the prediction horizon using a Taylor series expansion around $\bar{\mathbf{x}}_k$ and $\bar{\hat{\theta}}_k$ as follows:

$$\hat{E}_k^{\mathrm{c,app}} = \hat{E}_k^{\mathrm{c}}(\bar{\mathbf{x}}_k, \bar{\hat{\theta}}_k) + (\nabla \hat{E}_k^{\mathrm{c}}(\bar{\mathbf{x}}_k, \bar{\hat{\theta}}_k))^\top \begin{bmatrix} \mathbf{x}_k - \bar{\mathbf{x}}_k \\ \hat{\theta}_k - \bar{\hat{\theta}}_k \end{bmatrix}, \tag{15}$$

$$\hat{E}_k^{\mathrm{l,app}} = \hat{E}_k^{\mathrm{l}}(\bar{\mathbf{x}}_k, \bar{\hat{\theta}}_k) + (\nabla \hat{E}_k^{\mathrm{l}}(\bar{\mathbf{x}}_k, \bar{\hat{\theta}}_k))^\top \begin{bmatrix} \mathbf{x}_k - \bar{\mathbf{x}}_k \\ \hat{\theta}_k - \bar{\hat{\theta}}_k \end{bmatrix}. \tag{16}$$

We replace (15) and (16) in the objective function (13a) in the SPIC problem.

E. V2V Reformulation

As discussed in subsection II-F, ensuring collision avoidance requires the sets $\mathcal{P}_i$ and $\mathcal{P}_j$ to have no intersection, presenting a complex non-convex and non-smooth problem. To address this issue, the distance between these sets is used as the following primal problem [41]:

$$\mathrm{dist}(\mathcal{P}_i, \mathcal{P}_j) = \min_{\mathbf{p}_i, \mathbf{p}_j} \{\|\mathbf{p}_i - \mathbf{p}_j\|_2 \,|\, \mathbf{A}_i \mathbf{p}_i \leq \mathbf{b}_i, \mathbf{A}_j \mathbf{p}_j \leq \mathbf{b}_j\}, \tag{17}$$

with $\mathcal{P}_i = \{\mathbf{p}_i \in \mathbb{R}^2 \,|\, \mathbf{A}_i \mathbf{p}_i \leq \mathbf{b}_i\}$ and $\mathcal{P}_j = \{\mathbf{p}_j \in \mathbb{R}^2 \,|\, \mathbf{A}_j \mathbf{p}_j \leq \mathbf{b}_j\}$. To guarantee collision avoidance, not only the intersection of these sets should be empty, but also a minimum safe distance, d_s, must be kept in any direction between them, that is, $\mathrm{dist}(\mathcal{P}_i, \mathcal{P}_j) \geq d_\mathrm{s}$. The optimization problem (17) cannot be directly applied in the general form of the optimal control problem. The reason is that an optimization problem would act as a constraint for another optimization problem. To solve this problem, the duality theory is employed as suggested in [32], [41].

Given problem (17), where $\mathcal{P}_i$ and $\mathcal{P}_j$ are nonempty sets, the following dual problem can be solved instead of primal problem (17) as explained in [31], [32]:

$$\begin{aligned} \mathrm{dist}(\mathcal{P}_i, \mathcal{P}_j) = \max_{\boldsymbol{\lambda}_{i,j}, \boldsymbol{\lambda}_{j,i}, \mathbf{s}_{i,j}} \quad & -\mathbf{b}_i^\top \boldsymbol{\lambda}_{i,j} - \mathbf{b}_j^\top \boldsymbol{\lambda}_{j,i} \\ \text{s.t.} \quad & \mathbf{A}_i^\top \boldsymbol{\lambda}_{i,j} + \mathbf{s}_{i,j} = \mathbf{0},\ \mathbf{A}_j^\top \boldsymbol{\lambda}_{j,i} - \mathbf{s}_{i,j} = \mathbf{0}, \\ & \|\mathbf{s}_{i,j}\|_2 \leq 1,\ -\boldsymbol{\lambda}_{i,j} \leq \mathbf{0}, -\boldsymbol{\lambda}_{j,i} \leq \mathbf{0}, \end{aligned} \tag{18}$$

with $\boldsymbol{\lambda}_{i,j}, \boldsymbol{\lambda}_{j,i}$ and $\mathbf{s}_{i,j} = \mathbf{s}_{j,i}$ being the Lagrange multiplier vectors associated with the inequality constraints and equality constraints, respectively. Problem (18) can be reformulated as the following feasibility problem $\{\exists\ -\boldsymbol{\lambda}_{i,j} \leq \mathbf{0}, -\boldsymbol{\lambda}_{j,i} \leq \mathbf{0}, \mathbf{s}_{i,j} : -\mathbf{b}_i^\top \boldsymbol{\lambda}_{i,j} - \mathbf{b}_j^\top \boldsymbol{\lambda}_{j,i} \geq d_\mathrm{s}, \mathbf{A}_i^\top \boldsymbol{\lambda}_{i,j} + \mathbf{s}_{i,j} = \mathbf{0}, \mathbf{A}_j^\top \boldsymbol{\lambda}_{j,i} - \mathbf{s}_{i,j} = \mathbf{0}, \|\mathbf{s}_{i,j}\|_2 \leq 1\}$, using the intuition that the optimal value of the dual problem, which models the distance between $\mathcal{P}_i$ and $\mathcal{P}_j$, is constrained to be greater than d_s. This reformulation is used in place of the collision-avoidance constraint (13g) in the SPIC problem.

F. Final Formulation of the SPIC Problem

The final formulation of the SPIC problem involves (18) to address V2V collision avoidance constraints and applying the LTV approximation detailed in Section III-D. This approximation is applied to the basic problem formulation introduced in Section III-C, resulting in the following LTV-ENMPCC optimization problem:

$$
\begin{aligned}
\min_{\substack{\mathbf{u}_{i,\cdot|k},\nu_{i,\cdot|k},\\ \boldsymbol{\lambda}^{i,j}_{\cdot|k},\boldsymbol{\lambda}^{j,1}_{\cdot|k},\mathbf{s}^{i,j}_{\cdot|k}}} \quad & \sum_{i=1}^{N_\mathrm{v}} \left(\sum_{t=k}^{k+N_\mathrm{h}} \hat{\mathbf{E}}_{i,t}^{\mathrm{app}\,T} \mathbf{Q} \hat{\mathbf{E}}_{i,t}^{\mathrm{app}} - q_\theta \hat{\theta}_{i,t} \right. \\
& \left. + \sum_{t=k}^{k+N_\mathrm{h}-1} \mathbf{u}_{i,t}^\top \mathbf{R} \mathbf{u}_{i,t} + \nu_{i,t}^\top r_\nu \nu_{i,t} \right) \\
\text{s.t.} \quad & \mathbf{x}_{i,t+1|k} = \mathbf{A}_{i,t}\mathbf{x}_{i,t|k} + \mathbf{B}_{i,t}\mathbf{u}_{i,t|k} + \mathbf{d}_{i,t|k} \\
& \hat{\theta}_{i,t+1|k} = \hat{\theta}_{i,t|k} + \Delta t\, \nu_{i,t|k}, \\
& \mathbf{x}_{i,0|k} - \mathbf{x}_{i,k} = \mathbf{0},\ \hat{\theta}_{i,0|k} - \hat{\theta}_{i,k} = 0, \\
& \mathbf{x}_{i,t|k} \in \mathcal{X},\ \mathbf{u}_{i,t|k} \in \mathcal{U},\ \nu_{i,t|k} \in [0, \nu_{\max}], \\
& \left(-\mathbf{b}^i(\mathbf{x}^i_{t|k})^\top \boldsymbol{\lambda}^{i,j}_{t|k} - \mathbf{b}^j(\mathbf{x}^j_{t|k})^\top \boldsymbol{\lambda}^{j,i}_{t|k} \right) \geq d_\mathrm{s}, \\
& \mathbf{A}^i(\mathbf{x}^i_{t|k})^\top \boldsymbol{\lambda}^{i,j}_{t|k} + \mathbf{s}^{i,j}_{t|k} = \mathbf{0}, \\
& \mathbf{A}^j(\mathbf{x}^j_{t|k})^\top \boldsymbol{\lambda}^{j,i}_{t|k} - \mathbf{s}^{i,j}_{t|k} = \mathbf{0}, \\
& -\boldsymbol{\lambda}^{i,j}_{t|k} \leq \mathbf{0},\ -\boldsymbol{\lambda}^{j,i}_{t|k} \leq \mathbf{0},\ \|\mathbf{s}^{i,j}_{t|k}\|_2 \leq 1, \\
& \sqrt{(x^{\mathrm{ref}_i}(\hat{\theta}_{i,t|k}) - x_{i,t|k})^2 + (y^{\mathrm{ref}_i}(\hat{\theta}_{i,t|k}) - y_{i,t|k})^2} \\
& \leq \frac{w_\mathrm{r} - w_{\mathrm{v},i}}{2}.
\end{aligned} \tag{19}
$$

The complexity associated with problem (19) is reduced through the use of the LTV approximation of the nonlinear terms present in the objective function (13a) and the bicycle model (13b). Although LTV approximation of the V2V constraints can be a potential approach, for safety-critical constraints such as (13g) it is crucial to employ advanced methods that better capture the V2V constraints [42]. Accordingly, we mitigated the complexity of the V2V constraints by leveraging the duality theory. By this technique the non-differentiable collision avoidance constraints (13g) are reformulated into smooth and differentiable algebraic inequalities [41].

G. LTV-ENMPCC Algorithm

In this section, we present the LTV-ENMPCC algorithm to solve problem (19) and to simulate an intersection plaza in which CVAD continuously approach the intersection. The proposed algorithm leverages the ENMPCC method to efficiently compute optimal trajectories for each CVAD while considering various constraints. The LTV-ENMPCC algorithm is designed to handle dynamic scenarios in a random order, making it an ideal candidate for coordinating CVAD at the intersections where the vehicles are expected to interact with each other and with the intersection infrastructure. The main steps of the algorithm are summarized in Algorithm 1.

The algorithm starts assuming that no CVAD are in the intersection plaza. The algorithm then enters a loop and waits for the arrival of a CVAD at the intersection. As soon as a new CVAD arrives, its optimal inputs and state predictions are estimated according to its initial conditions, and then the number of CVAD, N_v, is incremented. These inputs and state predictions are used to compute the LTV approximation problem (19). For each CVAD, the lateral and longitudinal errors and the nonlinear dynamics around the estimated optimal inputs and state predictions are linearized.

Algorithm 1 LTV-ENMPCC Algorithm

Input: $N_\mathrm{v} = 0$, N_h, $\mathbf{x}_i(0)\ \forall i = 1, \ldots, N_\mathrm{v}$, $\mathbf{Q}$, $\mathbf{R}$

for $k = 0, 1, \ldots$ **do**
  if i-th CVAD arrived at the intersection **then**
    $N_\mathrm{v} \leftarrow N_\mathrm{v} + 1$
    Compute $\bar{\mathbf{u}}_{i,k}$ and $\bar{\nu}_{i,k}$ by using Procedure 1 introduced in [20].
    Compute $\bar{\mathbf{x}}_{i,k}$ and $\bar{\hat{\theta}}_{i,k}$ by applying $\bar{\mathbf{u}}_{i,k}$ and $\bar{\nu}_{i,k}$ to (1) and (5), respectively.
  end if
  for all $i = 1, \ldots, N_\mathrm{v}$ **do**
    Linearize $\hat{E}^\mathrm{c}_k$ and $\hat{E}^\mathrm{l}_k$ around $\bar{\mathbf{x}}_{i,k}$ and $\bar{\hat{\theta}}_{i,k}$, using (15) and (16).
    Linearize the nonlinear dynamics of the i-th CVAD (1), around $\bar{\mathbf{u}}_{i,k}$ and $\bar{\mathbf{x}}_{i,k}$ by using (14).
    Include the i-th CVAD in the new instance of the optimization problem (19).
  end for
  Solve the NLP optimization problem (19) and obtain $\mathbf{u}^*_{i,k}$, $\nu^*_{i,k}$.
  for all $i = 1, \ldots, N_\mathrm{v}$ **do**
    Update i-th CVAD states by applying the first element of $\mathbf{u}^*_{i,k}$ to the nonlinear dynamics (1).
    Update i-th CVAD progress by applying the first element of $\nu^*_{i,k}$ to (5).
    Compute $\bar{\mathbf{u}}_{i,k}$ and $\bar{\nu}_{i,k}$ by shifting optimal states and inputs predictions $\mathbf{u}^*_{i,k}$ and $\nu^*_{i,k}$.
    Compute $\bar{\mathbf{x}}_{i,k}$ and $\bar{\hat{\theta}}_{i,k}$ by applying $\bar{\mathbf{u}}_{i,k}$ and $\bar{\nu}_{i,k}$ to (1) and (5), respectively.
  end for
  if a CVAD left the intersection **then**
    Delete the CVAD from the NLP optimization problem (19).
    $N_\mathrm{v} \leftarrow N_\mathrm{v} - 1$
  end if
end for

Then, the CVAD is included in the instantiated NLP problem (19). The problem is solved and the optimal inputs for each CVAD are obtained. The algorithm then updates the state and progress of each CVAD using the computed optimal inputs and shifts the optimal inputs and states to estimate the next optimal inputs and state predictions. Finally, if a CVAD leaves the intersection, it is removed from the NLP problem in the next instance, and the number of CVAD in the system is decremented. The algorithm repeats this process for the remaining CVAD until the desired stopping criterion is reached.

H. Stability Analysis

To investigate the stability of the proposed method, we employ a technique based on contractive MPC [43], which ensures stability through the imposition of a contractive constraint. Contractive MPC has demonstrated its effectiveness in guaranteeing the closed loop stability in both linear time-varying MPC [44] and linear time-varying MPCC [20]. This

makes it particularly suitable for our application. We undertake the analysis with respect to a single vehicle, however, this analysis can be uniformly extended to the i-th CVAD, $i \in \mathcal{V}$. For simplicity, we omit the index i in the following.

To do so, we consider a change of coordinates:

$$\tilde{\mathbf{x}}_k = \mathbf{x}_k - \mathbf{x}^{\text{ref}}(\hat{\theta}_k), \tag{20}$$

with $\mathbf{x}^{\text{ref}}(\hat{\theta}) = [x^{\text{ref}}(\hat{\theta}), y^{\text{ref}}(\hat{\theta}), \psi^{\text{ref}}(\hat{\theta}), v^{\text{ref}}(\hat{\theta})]^\top$. Then, we define the following augmented nonlinear system

$$\begin{bmatrix}\tilde{\mathbf{x}}_{k+1}^T & \hat{\theta}_{k+1}\end{bmatrix}^\top = \tilde{\mathbf{f}}(\tilde{\mathbf{x}}_k, \hat{\theta}_k, \mathbf{u}_k, \nu_k), \tag{21}$$

where $\tilde{\mathbf{f}}(\cdot)$ is defined from (1), (5), and $\mathbf{x}^{\text{ref}}(\hat{\theta})$. Given that the origin of (21) serves as an equilibrium point, our objective hereafter is to ensure the stability of the origin of (21).

In contractive MPC, the contraction constraint remains constant for groups of N_h time steps. It is useful to express the time step $k = lN_\text{h} + m$, where $l \in \{0, 1, \ldots, \infty\}$ and $m \in \{0, 1, \ldots, N_\text{h} - 1\}$. Then, a norm of the state is constrained to decrease in order to enforce stability. The following norm is defined for $(\tilde{\mathbf{x}}, \hat{\theta})$ [43]:

$$\|\tilde{\mathbf{x}}, \hat{\theta}\|_V = \tilde{\mathbf{x}}^\top \mathbf{P} \tilde{\mathbf{x}} + p|\hat{\theta}|, \tag{22}$$

with $\mathbf{P}$ being a positive definite matrix and $p > 0$. The contraction constraint is subsequently defined in terms of $\|\cdot\|_V$ as:

$$\begin{aligned}&\|\tilde{\mathbf{x}}_{(l+1)N_\text{h}}, \hat{\theta}_{(l+1)N_\text{h}}\|_V \\ &\leq \begin{cases}\alpha\|\tilde{\mathbf{x}}_{lN_\text{h}}, \hat{\theta}_{lN_\text{h}}\|_V, & \text{if } \|\tilde{\mathbf{x}}_{lN_\text{h}}, \hat{\theta}_{lN_\text{h}}\|_V \leq \tilde{\alpha}, \\ \|\tilde{\mathbf{x}}_{lN_\text{h}}, \hat{\theta}_{lN_\text{h}}\|_V - \tilde{\alpha}, & \text{if } \|\tilde{\mathbf{x}}_{lN_\text{h}}, \hat{\theta}_{lN_\text{h}}\|_V > \tilde{\alpha},\end{cases}\end{aligned} \tag{23}$$

where $\alpha \in (0, 1)$ and $\tilde{\alpha} > 0$. Similar to [20], we approximate the contraction constraint (23) utilizing LTV approximation and impose it to the optimization problem (19). This formulation achieves the closed-loop stability of the system (21) as stated in [20, Theorem 1].

IV. Presentation and Discussion of Results

In this section, we present an evaluation of the LTV-ENMPCC algorithm for solving the optimization problem (19). Furthermore, we provide a comparison of the performance of the LTV-ENMPCC algorithm with that of the automated vehicles based on conventional path-based (lane-based) driving. The simulations are conducted on a Mac computer powered by an M1 chip and equipped with 8 GB of RAM. The LTV-ENMPCC algorithm is implemented in the Python programming language with CasADi [45]. To solve the corresponding NLP problem (19), we used Knitro [46]. The Knitro solver is employed with 8 threads for execution, utilizing multi-start capability. The splines for obtaining the reference paths were computed using the Python *spline* command.

A. Scenario Setup

The proposed method can be applied to any type of infrastructure, such as intersections of any geometry, roundabouts, and freeway on-ramp merges. We consider a challenging traffic scenario with the coordination of multiple vehicles entering the intersection plaza continuously. The simulations were conducted for a four-leg intersection illustrated in Fig. 1. This type of intersection is representative of real infrastructures worldwide and has been used in many previous works involving the coordination of CVAD at intersections [2], [11], [12]. In addition, this geometry enables a clear presentation of the method, including straight and turning movements, and two-way driving. A CVAD can approach the intersection plaza from four possible origins, namely south, north, west, or east, and can take one of three actions, turn left or right or go straight, i.e., toward any of the three remaining destinations. The six possible bidirectional reference paths that each CVAD can follow based on their entry and exit directions are displayed as colored dashed lines in Fig. 1.

Two simulation scenarios are considered. In Scenario 1 (SC1) we evaluate the LTV-ENMPCC algorithm described in Section III-G to generate collision-free trajectories for CVAD in a path-free intersection. In Scenario 2 (SC2) a conventional path-based (lane-based) driving of the CVAD is applied in the same conditions as SC1. In this scenario, we use the same SPIC problem formulation however, we use a tracking MPC objective function to provide a conventional path-based trajectory tracking problem as:

$$\begin{aligned}J = \sum_{i=1}^{N_\text{v}} \Bigg(&\sum_{t=k}^{k+N_\text{h}} q_\text{x}(x_{i,t} - x^{\text{ref}}(\hat{\theta}_{i,t}))^2 + q_\text{y}(y_{i,t} - y^{\text{ref}}(\hat{\theta}_{i,t}))^2 \\ &- q_\theta \hat{\theta}_{i,t} + \sum_{t=k}^{k+N_\text{h}-1} \mathbf{u}_{i,t}^\top \mathbf{R} \mathbf{u}_{i,t} + \nu_{i,t}^\top r_\nu \nu_{i,t} \Bigg)\end{aligned} \tag{24}$$

where q_x and q_y are suitable cost weights. We note that the reference paths are appropriately shifted to make a path-based scenario and no deviation from the paths is allowed. In SC2, the analysis is carried out on a two-lane intersection, where each vehicle is initially located in the center of each lane.

For each scenario, simulations of 900 time steps (180 s) with flows from 300 to 2100 veh/h/approach in steps of 600 veh/h/approach were tested. For each of these fifteen cases, seven replications with different seeds were run to obtain mean estimates of the performance metrics with 95% confidence of an error below 10% [47]. The vehicles are modeled with exact sizes, and no approximation is made. For convenience, it is also assumed that all the vehicles have uniform dimensions, but vehicles of different sizes could be considered simultaneously.

The arrival intervals between vehicles are generated randomly from a shifted negative exponential distribution [48]. The arrival position of the CVAD can be located at any arbitrary lateral position within the intersection boundaries. The arrival position along the road width at the entry point and the arrival speed around 15 m/s for each CVAD are randomly selected by sampling a uniform distribution. When exiting the plaza, the CVAD leave at either $x = 60$ m or $y = 60$ m, depending on the road used. Table II lists the other essential parameters of vehicles, intersection geometry, and the optimization problem.

TABLE II
SETTINGS FOR VEHICLES, INTERSECTION, AND OPTIMIZATION PROBLEM

Δt (s)	$v_{\max}$ (m/s)	$\delta_{\max}$ (rad)	$a_{\max}$ (m/s^2)	d_{s} (m)	w_{v} (m)	l_{v} (m)	l_{f} (m)	l_{r} (m)	w_{r} (m)	q_{c} (-)	q_{l} (-)	r_{v} (-)	r_{δ} (-)	q_{θ} (-)	r_{ν} (-)	$q_{\mathrm{x}}, q_{\mathrm{y}}$ (-)	N_{h} (steps)	N_{v} (-)
0.2	20	0.52	5	1	1.40	2.52	1.03	1.49	10	0.005	5	5	0.5	1	0.02	10	30	28

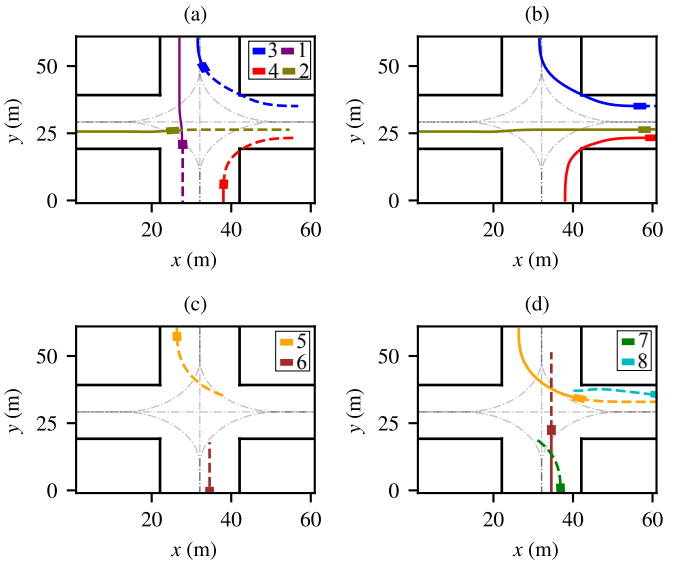

Fig. 5. SC1: snapshots of intersection plaza in time steps (a) 65, (b) 88, (c) 109, and (d) 130 operating under the LTV-ENMPCC algorithm with a flow of 1200 veh/h/approach.

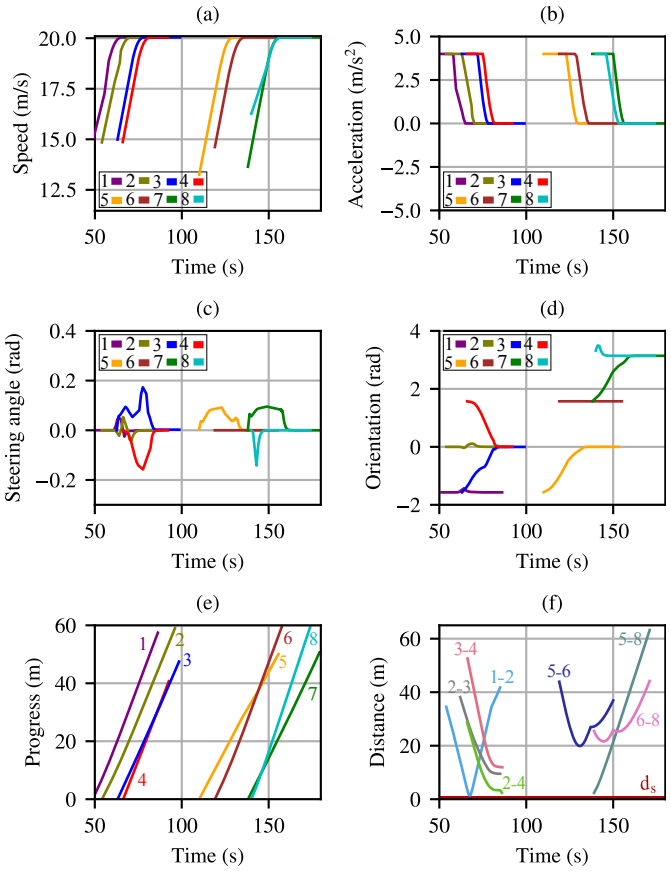

Fig. 6. SC1: states and inputs of the first eight vehicles in the intersection plaza operating under the LTV-ENMPCC algorithm with a flow of 1200 veh/h/approach.

B. Scenario 1 (SC1): The LTV-ENMPCC Algorithm in Action

Figure 5 shows a sequence of four snapshots of the application of the proposed LTV-ENMPCC algorithm with time steps 65, 88, 109, and 130. The flow is 1200 veh/h/approach. In the snapshots, the six gray dash-dotted lines show the reference paths for through, left, and right turning movements. The colored solid curves show the trajectories of the CVAD until the snapshot time step. The predicted trajectories for the next steps are shown by the dashed lines of the same color. New arrivals are included in a new instance of the problem. For example, vehicles 7 and 8 from Fig. 5(c) to Fig. 5(d). Vehicles that traveled beyond the exit point are removed in the next instance of the problem, for example, vehicle 1 from Fig. 5(a) to Fig. 5(b).

As depicted in Fig. 5, the vehicles have the ability to drive without being restricted to conventional path-related road lanes and horizontal markings. As a result, their trajectories may deviate from what would typically be expected using a path-based approach, to either maximize their progress or avoid potential collisions. Notably, the trajectories of vehicles 1 and 2 shown in Fig. 5(a), the trajectories of vehicles 3 and 4 depicted in Fig. 5(b), and the trajectories of vehicles 5 and 8 depicted in Fig. 5(d) serve as compelling examples of such deviations. Figure 5(b) illustrates the progress maximization achieved through the utilization of path deviation, leading to more effective utilization of the intersection space.

Furthermore, Fig. 5(a) provides an illustration of the collision avoidance constraint's effectiveness and the critical role played by the prediction horizon. Specifically, vehicles 1 and 2, traveling in straight paths, encountered a potential collision that was detected and addressed with a deviation from their original trajectories, as evidenced by the curved dashed lines in each predicted path. The executed paths, as shown in Fig. 5(b), confirm the avoidance maneuver taken by these vehicles. In addition, Fig. 5(d) provides evidence of the collision avoidance behavior of vehicle 8 upon entering the plaza, as it slightly deviates to the right of the road to prevent a collision with vehicle 5, which is exiting the plaza as evidenced by the curved dashed lines in the predicted path of vehicle 8.

To gain a better understanding of the snapshots, we can refer to Fig. 6 which displays the speed, acceleration, steering angle, orientation, and progress profiles of the vehicles depicted in Fig. 5 (vehicles 1–8) and the distances between selected vehicles. The vehicles accelerate to reach the maximum allowed speed and maintain that speed until they exit the intersection. To interpret the figures, we considered vehicle 8 as an example.

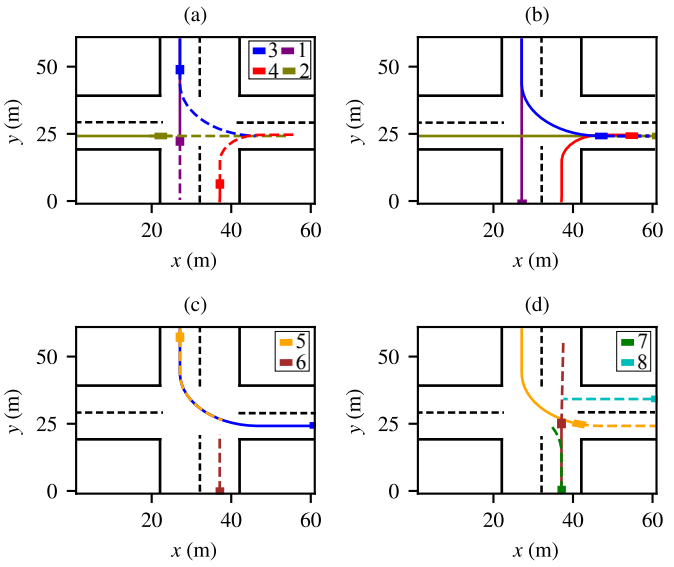

Fig. 7. SC2: snapshots of intersection plaza in time steps (a) 65, (b) 88, (c) 109, and (d) 130 operating under the conventional path-based control with a flow of 1200 veh/h/approach.

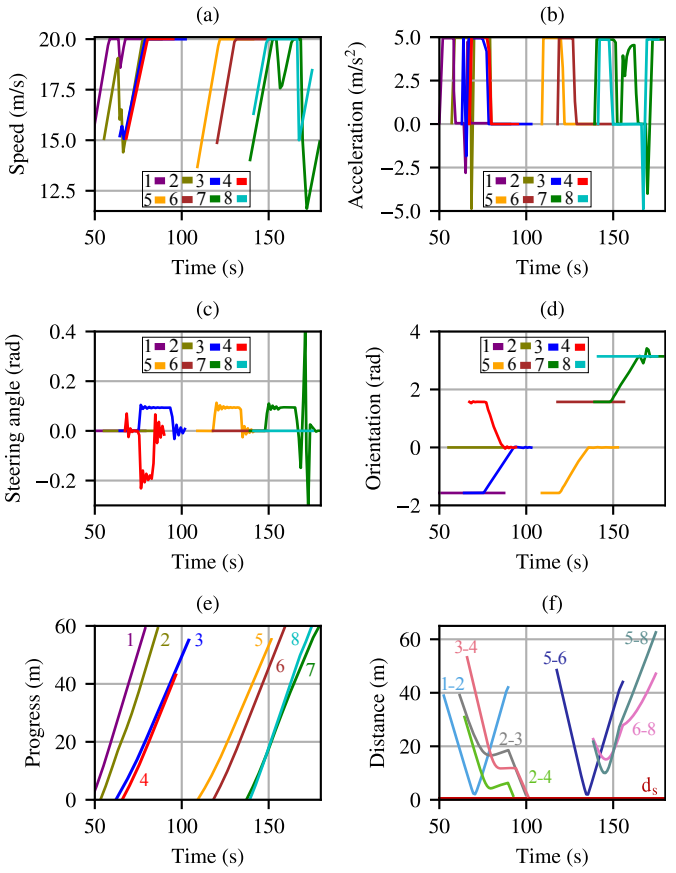

Fig. 8. SC2: states and inputs of the first eight vehicles in the intersection plaza operating under the conventional path-based control with a flow of 1200 veh/h/approach.

Vehicle 8 is seen to exhibit a slower rate of speed increase for a short period (Fig. 6(a)) and a reduction in its acceleration (Fig. 6(b)). Meanwhile, the vehicle is seen to steer to the right and then to the left (Fig. 6(c)) with corresponding temporary changes in their orientation (Fig. 6(d)). In addition, in Fig. 6(e) all vehicles have increasing progress profiles, which is one of this work's goals. Finally, Fig. 6(f) illustrates the distances between seven pairs of vehicles. As an example, it can be seen that the distance between vehicles 1 and 2 (the light-blue line) decreases and then increases staying above the minimum safe distance (the red line) to avoid a potential collision as shown in Figs. 5(a)–(b).

The obtained results demonstrate that the proposed method is able to produce collision-free multi-vehicle interaction and has the reasonable capability to resolve vehicle conflicts in challenging intersection scenarios.

C. Scenario 2 (SC2): Conventional Path-Based Approach

Figure 7 depicts four snapshots of the intersection plaza at the same time steps of the previous scenario and for the same seed. The corresponding states and control inputs of the vehicles, as well as the distance between selected vehicles in Fig. 7, are presented in Fig. 8. All vehicles are seen to increase their speed and acceleration once they enter the intersection. However, vehicles 1, 2, 3, 7, and 8 are seen to decrease their speed and acceleration for a short period to avoid a possible collision with other vehicles before accelerating and reaching the maximum allowed speed. This can potentially lead to vehicle delays and result in impaired traffic performance.

Vehicles 2 and 8 show a considerable reduction in their speed and acceleration to prevent a possible collision with vehicles 1 and 6, respectively, as illustrated in Figs. 8(a)–(b). In contrast, when using the LTV-ENMPCC algorithm, we see a smoother behavior of the vehicles, as depicted in Fig. 6(a)–(b), which is attributed to the path-free solution and the possibility of full use of the intersection space. This can affect the total time spent (TTS).

Furthermore, the distance traveled by the vehicles shown in Fig. 8(e) is longer compared to the path-free results illustrated in Fig. 6(e). This is because, in the path-based approach, the vehicles travel along the predefined reference paths and are not allowed to deviate from the paths, which can lead to inefficient use of the intersection space. To provide an illustration, consider vehicle 3 as an example. The LTV-ENMPCC algorithm generates a shorter path for vehicle 3 resulting in less traveled distance to exit the intersection as shown in Fig. 5(b) and Fig. 6(e). In the path-based scenario, however since vehicle 3 is not allowed to deviate from the predefined reference path, it traverses more distance to exit the intersection leading to longer vehicle progress as shown in Fig. 7(b) and Fig. 8(e). In general, the conventional path-based approach can lead to longer travel distances for vehicles, as it does not allow them to take advantage of all the available space in the intersection.

D. Total Time Spent (TTS)

Figure 9 shows the TTS for both the proposed LTV-ENMPCC method and the conventional path-based driving for various flow rates, ranging from 300 to 2100 veh/h/approach. The labels next to each box indicate the corresponding median

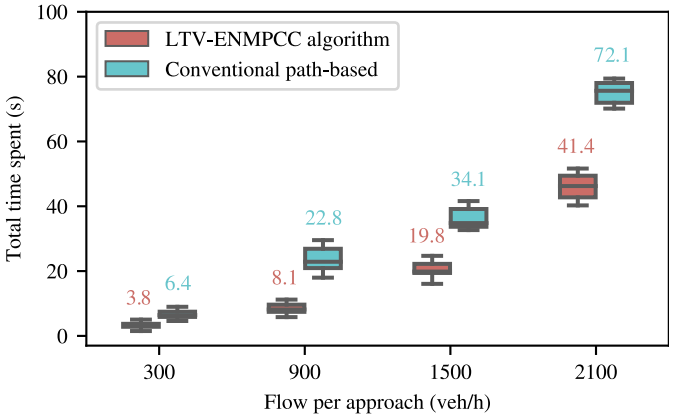

Fig. 9. The total time spent of SC1 (LTV-ENMPCC algorithm) and SC2 (conventional path-based) for flows from 300 to 2100 veh/h/approach. The numbers above each box provide the median values.

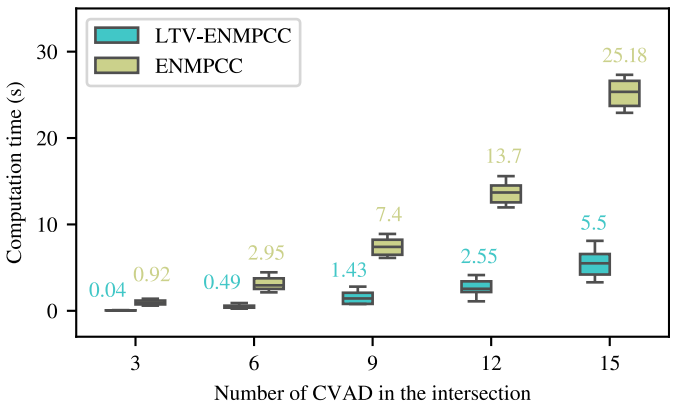

Fig. 10. The average computation time of the ENMPCC and LTV-ENMPCC methods for varying counts of CVAD numbers present in the intersection. The numbers above each box provide the median values.

TABLE III
AVERAGE FUEL CONSUMPTION (ML/S) OF SC1 (LTV-ENMPCC ALGORITHM) AND SC2 (CONVENTIONAL PATH-BASED)

Method \ Flow	300	900	1500	2100
LTV-ENMPCC algorithm	53.5	56.1	59.4	65.0
Conventional path-based	57.4	62.0	73.3	85.7

TTS values of each scenario. The TTS for both LTV-ENMPCC and ENMPCC methods do not have significant differences. Therefore, we do not show the TTS for the ENMPCC method in Fig. 9. By comparing the boxes within each flow rate category, one can observe that the LTV-ENMPCC algorithm generally results in a lower TTS. At all flow rates, the proposed method allows CVAD to follow free-path driving, resulting in lower TTS. Path-based driving may take longer due to tracking predefined paths and decelerating to avoid collisions, as shown in Figs. 6(a)–(b) and 8(a)–(b). As a result, the LTV-ENMPCC algorithm delivers a better performance and constitutes a more promising solution to enhance the overall efficiency of vehicular traffic at urban intersections.

E. Fuel Consumption

Finally, Table III presents the evaluation of the average fuel consumption of both LTV-ENMPCC algorithm and the conventional path-based approach. In this study, we adopt the fuel consumption model from [49], which assumes that a vehicle can be in four operational modes; idling, cruising at a constant speed, accelerating, and decelerating. The model uses different formulas to calculate the fuel consumption for each mode, and the parameters of the model are different for different vehicle engines. In the simulations, we use the parameters for the Honda Civic engine 1.8 L vehicle obtained from [50]. As can be seen from the table, the LTV-ENMPCC algorithm demonstrates lower fuel consumption than the conventional path-based method at all flow rates. The differences between the methods become more evident as the flow rate increases. This suggests that the LTV-ENMPCC algorithm might offer better fuel efficiency.

F. Computation Time (CT)

Figure 10 shows the average computation times for different numbers of CVAD at the intersection for seven runs of the proposed ENMPCC and LTV-ENMPCC methods. The labels next to each box indicate the corresponding median of the average computation times of each scenario. The computation time is relatively low when the number of vehicles is small, but it increases with the number of vehicles. Based on the results depicted in Fig. 10, it is evident that the LTV-ENMPCC method consistently outperforms the ENMPCC method in terms of average computation time across various numbers of vehicles in the intersection. This suggests that LTV-ENMPCC is more efficient regarding computational performance than ENMPCC. In the studied scenario, a demand of 1200 veh/h/approach results in a maximum of three vehicles in the intersection at the same time. Thus, with a computation time of 0.04 s for up to three vehicles, real-time operation is feasible in this case [18]. A trade-off between computation time and traffic performance can be worked out by tweaking optimization parameters, such as tolerance. Computation time could also be reduced by fixing the computed trajectories for vehicles already in the intersection, optimizing less often, or optimizing only for some vehicles. This is under investigation. Furthermore, leveraging the separable structure of the SPIC problem can lead to further improvement in computation time. Developing a distributed and parallel algorithm to exploit this structure is a potential avenue for future research.

G. LTV Approximation Accuracy

This section aims to demonstrate the impact of the LTV approximation on solution accuracy. Figure 11 illustrates the relative error across different prediction horizon lengths (N_{h}) ranging from 5 to 30. It is observed that as the prediction horizon increases, the relative error decreases. With $N_{\mathrm{h}} = 30$ utilized in the paper, Fig. 11 indicates a negligible relative error. Given that the difference in TTS of LTV-ENMPCC and ENMPCC is also negligible, as noted in Section IV-D, the results suggest that the approximation error resulting from

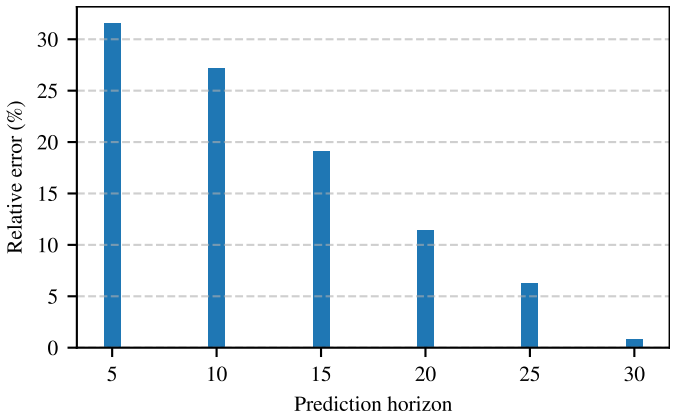

Fig. 11. LTV approximation relative error across various values of the prediction horizon.

LTV is acceptable considering the computational benefits it provides as shown in Fig. 10 compared to ENMPCC. In terms of safety-critical constraints, particularly collision avoidance constraints, we highlight that we did not linearize them. Instead, these non-differentiable constraints are reformulated into smooth, differentiable ones using duality theory, ensuring accuracy without compromising safety.

V. Conclusion

This paper proposed the signal-free path-free intersection control (SPIC) problem, which is a strategy for the coordination of connected vehicles under automated driving (CVAD) at urban intersections. SPIC offers a better use of the intersection space targeting to improve traffic efficiency and safety. In order to promote traffic safety, the SPIC problem uses a polytopic representation of CVAD and incorporates duality theory to satisfy V2V collision avoidance constraints. Additionally, a set of appropriate constraints to avoid collisions between CVAD and intersection plaza boundaries was introduced. An optimization-based receding horizon approach was introduced to address the SPIC problem solution. In particular, we proposed the LTV-ENMPCC algorithm which extends the standard nonlinear model predictive contouring control. The simulation results presented optimal and collision-free trajectories of CVAD with improved intersection space utilization, resulting in lower travel time and fuel consumption compared to the path-based driving approach.

Although the LTV-ENMPCC algorithm presented in this work offers some computational advantages over previous solutions, the computation time increases with the number of vehicles. Therefore, for higher demands, the solution time may not be small enough for real-time applications. Future research will focus on enhancing the SPIC formulation and its solution algorithm to achieve a better computation time. Furthermore, experimental evaluations in realistic scenarios will be considered.

References

[1] M. Papageorgiou, C. Diakaki, V. Dinopoulou, A. Kotsialos, and Y. Wang, "Review of road traffic control strategies," *Proceedings of the IEEE*, vol. 91, no. 12, pp. 2043–2067, 2003.

[2] L. Chen and C. Englund, "Cooperative intersection management: A survey," *IEEE Transactions on Intelligent Transportation Systems*, vol. 17, no. 2, pp. 570–586, 2016.

[3] J. Rios-Torres and A. A. Malikopoulos, "A survey on the coordination of connected and automated vehicles at intersections and merging at highway on-ramps," *IEEE Transactions on Intelligent Transportation Systems*, vol. 18, no. 5, pp. 1066–1077, 2017.

[4] A. Hadjigeorgiou and S. Timotheou, "Real-time optimization of fuel-consumption and travel-time of cavs for cooperative intersection crossing," *IEEE Transactions on Intelligent Vehicles*, vol. 8, no. 1, pp. 313–329, 2023.

[5] E. Ahmadi, R. C. Carlson, W. Kraus Junior, and E. Taheri, "Near-optimal coordination of vehicles at an intersection plaza using finite Fourier series," in *35º Congresso Nacional de Pesquisa e Ensino em Transportes*, Brasil, 2021.

[6] Z. He, L. Zheng, L. Lu, and W. Guan, "Erasing lane changes from roads: A design of future road intersections," *IEEE Transactions on Intelligent Vehicles*, vol. 3, no. 2, pp. 173–184, 2018.

[7] A. Zhou, S. Peeta, M. Yang, and J. Wang, "Cooperative signal-free intersection control using virtual platooning and traffic flow regulation," *Transportation Research Part C: Emerging Technologies*, vol. 138, p. 103610, 2022.

[8] S. D. Kumaravel, A. A. Malikopoulos, and R. Ayyagari, "Optimal coordination of platoons of connected and automated vehicles at signal-free intersections," *IEEE Transactions on Intelligent Vehicles*, vol. 7, no. 2, pp. 186–197, 2022.

[9] A. Stevanovic and N. Mitrovic, "Impact of conflict resolution parameters on combined alternate-directions lane assignment and reservation-based intersection control," *European Transport Research Review*, vol. 12, no. 1, p. 6, 2020.

[10] E. Ahmadi, R. C. Carlson, W. Kraus Junior, and E. Taheri, "Near-optimal coordination of vehicles at an intersection plaza using Bézier curves," in *The Eleventh International Conference on Advances in Vehicular Systems, Technologies and Applications*, Italy, 2022, pp. 6–12.

[11] B. Li, Y. Zhang, Y. Zhang, N. Jia, and Y. Ge, "Near-optimal online motion planning of connected and automated vehicles at a signal-free and lane-free intersection," in *IEEE Intelligent Vehicles Symposium*, China, 2018, pp. 1432–1437.

[12] M. Amouzadi, M. O. Orisatoki, and A. M. Dizqah, "Optimal lane-free crossing of CAVs through intersections," *IEEE Transactions on Vehicular Technology*, vol. 72, pp. 1488–1500, 2022.

[13] R. C. Carlson, E. Ahmadi, E. R. Müller, and G. W. S. d. Silva, "Optimal coordination of connected vehicles under automated driving at path-free signal-free urban intersections," in *36º Congresso Nacional de Pesquisa e Ensino em Transportes*, Brasil, 2022.

[14] E. Ahmadi and R. C. Carlson, "Model predictive control of multi-vehicle interaction at unsignalized intersections," in *36º Congresso Nacional de Pesquisa e Ensino em Transportes*, Brasil, 2022.

[15] M. Sekeran, M. Rostami-Shahrbabaki, A. A. Syed, M. Margreiter, and K. Bogenberger, "Lane-free traffic: History and state of the art," in *IEEE 25th International Conference on Intelligent Transportation Systems (ITSC)*, 2022, pp. 1037–1042.

[16] B. Li, Y. Zhang, N. Jia, and X. Peng, "Autonomous intersection management over continuous space: A microscopic and precise solution via computational optimal control," *IFAC-PapersOnLine*, vol. 53, no. 2, pp. 17 071–17 076, 2020.

[17] E. Ahmadi and R. C. Carlson, "Model predictive control of connected vehicles under automated driving at path-free signal-free intersections," *Transportes*, vol. 31, no. 3, pp. e2880–e2880, 2023.

[18] R. Levy and J. Haddad, "Cooperative path and trajectory planning for autonomous vehicles on roads without lanes: A laboratory experimental demonstration," *Transportation Research Part C: Emerging Technologies*, vol. 144, p. 103813, 2022.

[19] E. R. Müller, R. C. Carlson, and W. Kraus, "Time optimal scheduling of automated vehicle arrivals at urban intersections," in *19th IEEE International Conference on Intelligent Transportation Systems*, Brazil, 2016, pp. 1174–1179.

[20] D. Lam, C. Manzie, and M. Good, "Model predictive contouring control," in *49th IEEE Conference on Decision and Control*. IEEE, 2010, pp. 6137–6142.

[21] A. Liniger, A. Domahidi, and M. Morari, "Optimization-based autonomous racing of 1:43 scale RC cars," *Optimal Control Applications and Methods*, vol. 36, no. 5, pp. 628–647, 2015.

[22] V. K. Yanumula, P. Typaldos, D. Troullinos, M. Malekzadeh, I. Papamichail, and M. Papageorgiou, "Optimal trajectory planning for connected and automated vehicles in lane-free traffic with vehicle nudging,"

IEEE Transactions on Intelligent Vehicles, vol. 8, no. 3, pp. 2385–2399, 2023.
[23] M. Naderi, M. Papageorgiou, D. Troullinos, I. Karafyllis, and I. Papamichail, "Controlling automated vehicles on large lane-free roundabouts," *IEEE Transactions on Intelligent Vehicles*, vol. 9, no. 1, pp. 3061–3074, 2024.
[24] B. Li, Y. Zhang, T. Acarman, Y. Ouyang, C. Yaman, and Y. Wang, "Lane-free autonomous intersection management: A batch-processing framework integrating reservation-based and planning-based methods," in *IEEE International Conference on Robotics and Automation*, China, 2021, pp. 7915–7921.
[25] B. Siciliano and O. Khatib, Eds., *Springer Handbook of Robotics*. Berlin, Heidelberg: Springer, 2008.
[26] A. G. Ulsoy, H. Peng, and M. Cakmakci, *Automotive Control Systems*. Cambridge: Cambridge University Press, 2012.
[27] J. Kong, M. Pfeiffer, G. Schildbach, and F. Borrelli, "Kinematic and dynamic vehicle models for autonomous driving control design," in *IEEE Intelligent Vehicles Symposium*, 2015, pp. 1094–1099.
[28] Y. Koren and C.-C. Lo, "Variable-gain cross-coupling controller for contouring," *CIRP Annals*, vol. 40, no. 1, pp. 371–374, 1991.
[29] H. Wang, J. Kearney, and K. Atkinson, "Arc-length parameterized spline curves for real-time simulation," in *Proc. 5th International Conference on Curves and Surfaces*, vol. 387396, 2002.
[30] N. M. Patrikalakis and T. Maekawa, *Shape Interrogation for Computer Aided Design and Manufacturing*. Springer, 2002, vol. 15.
[31] R. Firoozi, X. Zhang, and F. Borrelli, "Formation and reconfiguration of tight multi-lane platoons," *Control Engineering Practice*, vol. 108, p. 104714, 2021.
[32] X. Zhang, A. Liniger, and F. Borrelli, "Optimization-based collision avoidance," *IEEE Transactions on Control Systems Technology*, vol. 29, no. 3, pp. 972–983, 2020.
[33] T. Faulwasser, B. Kern, and R. Findeisen, "Model predictive path-following for constrained nonlinear systems," in *Proceedings of the 48th IEEE Conference on Decision and Control held jointly with the 28th Chinese Control Conference*, 2009, pp. 8642–8647.
[34] Y. Koren and C.-C. Lo, "Advanced controllers for feed drives," *CIRP Annals*, vol. 41, no. 2, pp. 689–698, 1992.
[35] J. Rossiter, *A First Course in Predictive Control*. CRC Press, 2018.
[36] E. Gilbert and I. Kolmanovsky, "Nonlinear tracking control in the presence of state and control constraints: a generalized reference governor," *Automatica*, vol. 38, no. 12, pp. 2063–2073, 2002.
[37] N. Li, D. W. Oyler, M. Zhang, Y. Yildiz, I. Kolmanovsky, and A. R. Girard, "Game theoretic modeling of driver and vehicle interactions for verification and validation of autonomous vehicle control systems," *IEEE Transactions on Control Systems Technology*, vol. 26, no. 5, pp. 1782–1797, 2017.
[38] W. Schwarting, J. Alonso-Mora, L. Paull, S. Karaman, and D. Rus, "Safe nonlinear trajectory generation for parallel autonomy with a dynamic vehicle model," *IEEE Transactions on Intelligent Transportation Systems*, vol. 19, no. 9, pp. 2994–3008, 2018.
[39] T. Nägeli, L. Meier, A. Domahidi, J. Alonso-Mora, and O. Hilliges, "Real-time planning for automated multi-view drone cinematography," *ACM Transactions on Graphics (TOG)*, vol. 36, no. 4, pp. 1–10, 2017.
[40] P. Falcone, F. Borrelli, J. Asgari, H. E. Tseng, and D. Hrovat, "Predictive active steering control for autonomous vehicle systems," *IEEE Transactions on Control Systems Technology*, vol. 15, no. 3, pp. 566–580, 2007.
[41] S. Boyd and L. Vandenberghe, *Convex Optimization*. Cambridge University Press, 2004.
[42] S. E. Li, Z. Wang, Y. Zheng, Q. Sun, J. Gao, F. Ma, and K. Li, "Synchronous and asynchronous parallel computation for large-scale optimal control of connected vehicles," *Transportation Research Part C: Emerging Technologies*, vol. 121, p. 102842, 2020.
[43] S. L. de Oliveira Kothare and M. Morari, "Contractive model predictive control for constrained nonlinear systems," *IEEE Transactions on Automatic Control*, vol. 45, no. 6, pp. 1053–1071, 2000.
[44] S. L. de Oliveira, "Model predictive control (MPC) for constrained nonlinear systems," Ph.D. dissertation, California Institute of Technology, 1996.
[45] J. A. Andersson, J. Gillis, G. Horn, J. B. Rawlings, and M. Diehl, "CasADi – a software framework for nonlinear optimization and optimal control," *Mathematical Programming Computation*, vol. 11, no. 1, pp. 1–36, 2019.
[46] R. H. Byrd, J. Nocedal, and R. A. Waltz, "KNITRO: An integrated package for nonlinear optimization," *Large-scale Nonlinear Optimization*, pp. 35–59, 2006.
[47] A. M. Law, *Simulation Modeling and Analysis*, 5th ed. Dubuque: McGraw-Hill Education, 2013.
[48] FHWA. Traffic Analysis Toolbox Volume III: Guidelines for Applying Traffic Microsimulation Modeling Software. [Online]. Available: https://ops.fhwa.dot.gov/trafficanalysistools/tat_vol3/sectapp_a.htm
[49] R. Akçelik, "Progress in fuel consumption modelling for urban traffic management." Australian Road Research Board Melbourne, Australia, 1983.
[50] A. T. Marinho, R. A. L. Eccel, R. C. Carlson, and W. K. Junior, "Calibração do modelo de consumo de combustível do simulador AIMSUN com dados coletados via OBD," *Transportes*, vol. 26, no. 2, pp. 139–154, 2018.

Elham Ahmadi received the M.Sc. degree in electrical and electronics engineering from the Shiraz University of Technology (SUTCH), Iran, in 2017, and Ph.D. degree in automation and system engineering from the Federal University of Santa Catarina (UFSC), Brazil in 2023. She is currently a postdoctoral researcher at the University of Vaasa, Finland. Her research interests include mathematical optimization, control theory, estimation, and machine learning with applications to navigation and autonomous systems.

Alireza Olama received his M.Sc. in control engineering from Shiraz University of Technology (SUTECH), Iran, in 2017 and completed his Ph.D. in automation and systems engineering at the Federal University of Santa Catarina (UFSC), Brazil, in 2023. He has been with the information technology department at Åbo Akademi University, Finland since 2023 where his areas of research encompass model predictive control, computational optimization, distributed and federated learning, and software engineering.

Rodrigo C. Carlson received the Bel.Eng. degree in control and automation engineering and the M.E. degree in electrical engineering from the Federal University of Santa Catarina (UFSC), Brazil, in 2004 and 2006, respectively, the B.B.A. degree in business administration from the Santa Catarina State University, Brazil, in 2006, and the Ph.D. degree from the Technical University of Crete, Greece, in 2011. From 2012 to 2015, he was with the Mobility Engineering Center and since 2015 he has been with the Department of Automation and Systems at UFSC. His research interests are control and optimization applications to traffic systems.

Eduardo Camponogara (M'07) received a Ph.D. in electrical and computer engineering from Carnegie Mellon University, USA, in 2000. After being a postdoctoral fellow at the Institute for Complex Engineered Systems, USA, he joined the Department of Automation and Systems Engineering faculty at the Federal University of Santa Catarina, Brazil, in 2002. His research interests include systems optimization, distributed decision-making, and traffic control engineering.